INTERNATIONAL JOURNAL OF ENGINEERING RESEARCH
Volume 2, Issue 1, 2025

PHOTOCATALYTIC DEGRADATION OF ORGANIC POLLUTANTS VIA METAL-OXIDE NANOSTRUCTURES

Muhammad Zeshan Azam

Department of Chemical Engineering, Wah Engineering College, University of Wah, 47040, Pakistan

itszeshanazam757@gmail.com

Keywords
Metal-oxide nanostructures, Organic pollutant degradation, Wastewater treatment, Photo catalysis

Article History
Received: 01 January, 2025
Accepted: 21 February, 2025
Published: 31 March, 2025

Corresponding Author: *
Muhammad Zeshan Azam

Abstract
Increasing contamination of freshwater by persistent organic pollutants calls for efficient and eco-friendly treatment methods. This study explores photocatalytic degradation of organic dyes using metal-oxide nanostructures (TiO_2, ZnO, Fe_2O_3) synthesized via sol-gel and hydrothermal techniques. Characterization by SEM, FTIR, XRD, and UV-Vis confirmed well-dispersed nanostructures with favorable structural and optical properties. Under UV and visible light, significant degradation of dyes like methylene blue, Rhodamine B, and methyl orange was observed. Photocatalytic efficiency was tested across catalyst dosage, dye concentration, pH, and light conditions. Kinetic analysis indicated pseudo-second-order behavior, suggesting surface chemisorption as the key degradation mechanism. Reusability tests showed catalyst stability over multiple cycles. These results demonstrate the potential of green-synthesized metal-oxide nanostructures as sustainable catalysts for effective wastewater treatment.

INTRODUCTION

Environmental pollution is increasing day by day and imposing severe and irreversible damage to the world. It is of different types: air, water, soil, noise, light, etc. Urbanization and technological development have put the survival of the planet in danger by degrading the quality of the environment's essential elements air, water and soil due to the release of hazardous waste from factories like plastics, heavy metals, nitrates, burning of fossil fuels, acid rain, oil spills and industrial toxins. Urbanization and overpopulation have increased city noise and light pollution. Polluting agents are exponentially increasing in modern society, disturbing the ecological balance and posing extinction problems for different animal and bird species. This is because the destruction of plants, especially trees, by acid rains disturbs the natural environment of animals [1]. Water is the most valuable reserve among all natural assets present on the Earth. Earth is recognized as a blue planet because of the occurrence of plentiful water on its surface [2]. Owing to its exclusive structure and characteristics, water is taken as a matrix of life [3]. It is projected that 97.3% of the whole water present on the earth is saline. The entire freshwater which is only 2.7% of whole water, approximately 68% is frozen in form of ice and glaciers 30% as groundwater and leftover [4] about 1.3% is found on the surface of the earth in lake and rivers C.G.W.M. 1990.Freshwater, especially is very important in context to sustenance as it is required for household consumption and also as industrial and farming use. The water applied for human utilization should be "safe and wholesome" i.e. odorless, colorless, and fine in taste and liberated from dangerous chemical agents and pathogen [5].

The quality of water being used is, however, an important issue as a decrease in quality of water reduces its utility for a human being and other organisms [6]. Industrial use of toxic, water-soluble dyes especially in textile, food, leather, and paper industries is a major source of environmental pollution [7]. Untreated effluents contaminate soil and water, affecting human health through the food chain. Everyday products like colored paper and towels also contribute to exposure [8]. These dyes are often carcinogenic and mutagenic.

Water pollution also stems from pathogens introduced through sewage and industrial discharge. Microorganisms like E. coli, coliforms, and various bacteria can cause diseases such as cholera, typhoid, and hepatitis [9]. Fecal contamination introduces harmful microbes, especially in stagnant water.

Suspended solids SS, both organic and inorganic, further affect aquatic life by blocking sunlight and damaging fish gills [10]. The impact depends on SS concentration, exposure time, and particle size [11]. Physical, chemical, and biological processes are the primary elements of conventional wastewater treatment techniques. While physical methods like sedimentation and filtration work well for eliminating suspended solids, they are not enough to dissolve organic contaminants [12]. While chemical treatments such as ozonation, chlorination, and coagulation can neutralize contaminants, they frequently produce hazardous byproducts, secondary pollution, and high operating costs [13]. Although biological methods like trickling filters and activated sludge rely on microbial degradation, they are usually slow and inefficient when dealing with complex or non-biodegradable organic compounds. In addition, all of these techniques usually result in the production of substantial amounts of sludge, which requires additional processing and secure disposal [14]. These drawbacks highlight the need for more sophisticated, efficient, and environmentally friendly substitutes, like photocatalysis, which can provide total pollution degradation with little adverse effects on the environment [15].

Water resource is the most precious resource for a human being that it is necessary to make the water resource to be clean and also non-toxic. Anyway, due to urbanization, industrialization, and lack of people awareness to consider water as a crucial commodity, people in many countries are now facing problems related to water supply and security [16]. Presently, water pollution becomes one of the most serious global issues, especially, water pollutions that contaminate various types of organic compounds [17], including pharmaceuticals and personal care products, persistent organic pollutants, and organic dyes.In recent years, many researchers have developed the remediation techniques of organic pollutants in water. Photo catalysis, as one of the advanced oxidation processes AOPs using reactive oxidative radicals or species, particularly hydroxyl radicals, to remediate the organic pollutants, has drawn much attention recently.Various types of photocatalysis can be considered to be a green and effective strategy for solving global environmental and energy problems. The possibility to utilize solar energy as a free energy from nature to solve the environmental problems is the key significance of photocatalysis. Photocatalysis is a type of catalysis which a chemical reaction is accelerated in the presence of a catalyst so-called photocatalyst on exposure to light which is mostly described in term of photon hν – an elementary particle of light, where the photocatalyst participates in the chemical reaction without being consumed. Photocatalysis can be also defined as the acceleration of a photoreaction e.g., photolysis in the presence of a catalyst. There are various types of pollutants in wastewater e.g., organic pollutants, inorganic pollutants, pathogens, and radioactive pollutants. Organic pollutants are a main part of environmental pollution, which may cause an adverse effect on aquatic organisms even at low levels of exposure [18].Organic pollutants are found in various wastewater sources, e.g., domestic, industrial, and agricultural sectors. Many kinds of organic pollutants, such as pharmaceuticals and personal care products PPCPs, textile, food, beverage, persistent organic pollutants POPs, insecticide, pesticide, oil, fertilizers, and chemical, are included in wastewater [19].

Nanotechnology has also proven to be one of the most advanced and best strategies for wastewater treatment. NP has high interaction, adsorption, and reactivity due to its small size and high surface-atom ratio [20].

They were suspended within hydrous solutions to act as colloids. These particles save energy due to their small size, which can ultimately lead to cost-effectiveness. NPs have a great advantage in treating water at great depths and in any place that has not been cleaned by conventionally available procedures [21]. Green nanomaterials are more likely to treat water contaminated with toxic metal ions, inorganic solutes, and organic and pathogenic microorganisms. Advanced research and commercialization of different nanomaterials nanostructured catalytic membranes, nano-absorbents, biologically active NPs, nano-catalysts, biomimetic membranes, and molecularly imprinted polymers MIP were performed to remove pathogenic bacteria, toxic metal ions, organic solutes, and inorganic substances from water [22]. The widespread usage of pesticides in the field of agriculture has had a significant impact on human health and the environment because these pollutants are not properly removed from the water. Pesticides also can have adverse effects on aquatic animals and humans because they are not completely removed from the aquatic environment by conventional wastewater treatment methods. Thus, processes such as heterogeneous photocatalysis and nano-composite adsorption have received considerable interest within the scientific society due to their unique properties, in addition to their ability to degrade and remove certain substances such as organic pollution, including pesticides [23].Existing metal-oxide nanostructures still have a number of disadvantages, despite increased interest in the photocatalytic degradation of organic pollutants. Due to rapid charge carrier recombination and limited light absorption, commonly used photocatalysts like ZnO and TiO_2 frequently behave poorly in visible light. In addition, a lot of methods for synthesis use hazardous substances, which raises environmental issues. In addition, little is known about how structural characteristics such as particle size, surface area, and morphology affect photocatalytic efficiency. Furthermore, tiny is known about these materials' long-term stability, recyclability, and practicality. In light of this, the current study attempts to evaluate the structural, morphological, and optical properties of environmentally friendly metal-oxide nanostructures by integrating them using inexpensive strategies. In order to understand the impact of operational parameters, the photocatalytic performance will be evaluated under various kinds of circumstances. In order assist in developing of environmentally friendly wastewater treatment methods, the study also aims to examine the mechanism of degradation and evaluate the catalysts' reusability. In order to assist in the creation of environmentally friendly wastewater treatment methods, the study also indicates to examine the mechanism of degradation along with assessing the catalysts' reusability.

2 Materials and methods

2.1 Chemicals and Reagents

Each substance used in this investigation was analytical grade and didn't require any further purification. We purchased metal precursors from Sigma-Aldrich, which includes ironIII nitrate nonahydrate $FeNO_{33}\cdot 9H_2O$, zinc nitrate hexahydrate $ZnNO_{32}\cdot 6H_2O$, and titaniumIV isopropoxide TTIP. To evaluate photocatalytic degradation, organic dye pollutants such as methyl orange MO, rhodamine B RhB, and methylene blue MB were selected as model organic pollutants. Ethanol C_2H_5OH, deionized water DI, hydrochloric acid HCl, and sodium hydroxide NaOH were additional reagents employed for pH modification.

2.2 Synthesis of Metal-Oxide Nanostructures

Because of their simplicity of utilization and ability for producing nanomaterials with huge surface areas as well as controlled morphology, the sol-gel and hydrothermal methods were employed for generating different metal-oxide nanostructures.

2.2.1 Sol-Gel Synthesis of TiO_2 Nanoparticles

Sol-gel was used to produce titanium dioxide TiO_2 nanoparticles. In short, 100 mL of ethanol was stirred constantly whereas 20 mL of titanium isopropoxide was dissolved. The precursor was stirring constantly while a separate solution of deionized water and ethanol 1:1 v/v was added dropwise. To generate crystalline TiO_2 nanoparticles, the resulting white gel was aged for 24 hours, dried at 80°C, and then calcined for 3 hours at 450°C.

Ajay Sharma 2014 stated that the nanostructures TiO2 exists in three polymorphic phase viz. rutile, anatase and brookite. Amongst these three, anatase & rutile are most thermally stable phases of TiO2. Anatase structure of TiO2 belongs to D14 4h-P42/mnm space group lattice constant a = 0.4584 nm, c = 0.2953 nm, c/a = 0.664, while rutile structure belongs to D19 4h-I41/amd space group lattice constant a = 0.3733 nm, c = 0.937 nm, c/a = 2.51 [24]. These two structures have great importance in the preparation of dssc, due to its high surface area. TiO2 nanoparticles adsorb more amounts of dye molecules, which results into the increase photon to current conversion efficiency, because a TiO2 nanoparticles-coated photoelectrode usually has higher transparency, which cause to transmission of a significant amount of visible light, the smaller particle size of the TiO2 nanoparticles only permits negligible amount of light scattering [25]. The several methods for preparation of nanocrystallite titania are well reported, most of them belonging to wet chemical method. The benefits of the wet chemical method are well studied [26]. The best choices of wet chemical methods are hydrothermal and sol–gel [27]. The Sol–gel method is the simple, economical, and accomplished and most frequently used methods of synthesizing TiO2 nanoparticles. The sol–gel method gives accessibility for synthesizing TiO2 nanoparticles with different morphologies like sheets, tubes, particles, wires, rods, mesoporous and aerogels. The nano-structured TiO2 has been synthesized by the hydrolysis process of Titanium IV Isopropoxide. The thin films were prepared by dip coating method. The crystallite size of as prepared TiO2 nanoparticles was obtained approximately 20 nm and anatase and rutile phases confirmed by XRD graph. FE-SEM was employed to further study of the crystallite/particle size and morphology of the as-synthesized TiO2 particles. The particles of TiO2 in anatase phase have a mostly spherical morphology. The optical absorbance of the prepared films was found between 360 nm to 310 nm which is correspond to the band gap of TiO2 ~3.2 ev. From the DSC-TGA analysis phase transformation of TiO2 obtained at 720 °C. From I-V graph efficiency was achieved about 1.77 % [28].

2.2.2 Hydrothermal Synthesis of ZnO Nanostructures

In order to produce ZnO nanostructures, 5 g of zinc nitrate hexahydrate was dissolved in 50 mL of deionized water and mixed with 5 mL of 1 M NaOH solution while stirring constantly. subsequently that, the mixture that was homogenous was put into an autoclave lined with Teflon and heated to 150°C for 12 hours. After being frequently sterilized with ethanol and water, the product was dried at 80°C. To enhance crystallinity, the powder was ultimately calcined for two hours at 500°C.

Vjaceslavs Gerbreders et al 2020 demonstrated that amongst the most popular methods for the production of metal oxide nanostructures is hydrothermal synthesis. For producing ZnO nanostructures, a nitrate-based precursor reaction with equimolar amounts of hexamethylenetetramine HMTA is commonly used. In these reactions, zinc nitrate provides the source of Zn^{2+} ions, and HMTA produces the desired amount of OH^- ions. The growth process occurs due to a dissolution-secondary precipitation mechanism. ZnO nanostructures are characterized by anisotropic growth with different growth rates of the individual faces, where $v0001 > v10\bar{1}0 > v10\bar{1}\bar{1} > v10\bar{1}1 > v000\bar{1}$. Therefore, considering the principle of energy minimization, the most favorable is vertical growth perpendicular to the 0001 plane, which ensures the formation of characteristic rod-like nanostruchtures of ZnO. The mentioned process takes place when chemical reactions are in equilibrium. Shifting from the equilibrium conditions by varying the parameters of reaction, or using capping agents, makes it possible to change the growth rate of individual crystallographic planes and, as result, affect the morphology of the obtained nanostructure [29].

2.2.3 Synthesis of Fe_2O_3 Nanoparticles

For the purpose of to produce iron oxide FeO_3 nanoparticles, 2 g of ironIII nitrate was immersed in 50 mL of deionized water, and 10 mL of ammonia solution was added dropwise until pH 8 was obtained. After two hours of mixing at room temperature, the mixture was left to age for a whole night. After being

sterilized and dried at 100°C, the precipitate was calcined for three hours at 400°C.

Antara R. Chakraborty et al. 2024 demonstrated that Iron oxide nanoparticles were synthesized via a chemical co-precipitation method, involving several sequential steps. Initially, 6.7 g of FeCl3.6H2O was dissolved in 100 mL of distilled water to form a solution. Subsequently, the solution was subjected to chemical bath deposition, where it was stirred vigorously at room temperature. The next step involved the gradual addition of NH4OH dropwise to the stirring mixture, resulting in the formation of a black dispersion. This dispersion was continuously stirred for 1 h to ensure homogeneity. Following this, the solution was heated to 80 ◦C for 2 h to facilitate evaporation, after which it was cooled to room temperature and left undisturbed for 5 days to allow precipitation of iron oxide. The precipitated iron oxide was collected using filter paper, and this process was repeated to obtain six samples. These samples were then subjected to an annealing process at different temperatures: annealed, 100 ◦C, 300 ◦C, 500 ◦C, 700 ◦C, and 900 ◦C. After annealing, the samples were ground into fine powders for further characterization. During the synthesis of iron oxide nanoparticles, the reaction pH played a crucial role in determining the efficiency and outcome of the co-precipitation process. In the initial steps, a solution of 6.7 g of $FeCl_3 \cdot 6H_2O$ in 100 mL of distilled water was prepared. To this, ammonium hydroxide NH_4OH was added dropwise, and the pH of the reaction mixture was closely monitored. The addition of NH_4OH gradually increased the pH to approximately 9, which is slightly alkaline. This pH was maintained to ensure optimal conditions for the precipitation of ferric hydroxide $FeOH_3$, a precursor to iron oxide nanoparticles Fe_2O_3. Maintaining this pH ensures that the reaction proceeds efficiently, favoring the nucleation and growth of uniform nanoparticles, and minimizing unwanted side reactions. The controlled pH of 9 created optimal conditions for the formation of ferric hydroxide nuclei, which subsequently underwent dehydration and oxidation, leading to the formation of Fe_2O_3 nanoparticles. The nanoparticles NPs were annealed at specific temperatures to control their crystallinity, phase transitions, and magnetic properties. Annealing at lower temperatures 100 ◦C–300 ◦C facilitates the transition from amorphous or poorly crystalline phases to more defined crystalline structures, such as the γ-Fe_2O_3 maghemite phase. Higher annealing temperatures 500 ◦C–900 ◦C promote the phase transition from γ-Fe_2O_3 to α-Fe_2O_3 hematite, enhancing the crystallinity and magnetic properties of the nanoparticles. The selection of these specific temperatures ensures optimal control over the structural and magnetic characteristics of the synthesized nanoparticles, aligning with the goals of the study to produce NPs with desirable properties for various applications. Characterization of the synthesized products was performed using various techniques, including Scanning Electron Microscopy SEM, X-Ray Diffraction XRD, Fourier Transform Infrared Spectroscopy FTIR, Zita potential, dynamic light scattering and UV–Vis Spectroscopy. These techniques allowed for the differentiation between unannealed and annealed products, providing valuable insights into their structural and chemical properties [29].

3 Results and discussion

3.1 SEM

The synthesized metal-oxide nanostructures have a uniform and well-dispersed morphology, generally spherical, rod-like, or flower-like depending on the synthesis route, according to SEM images. This consistency indicates defined synthesis-related nucleation and growth.

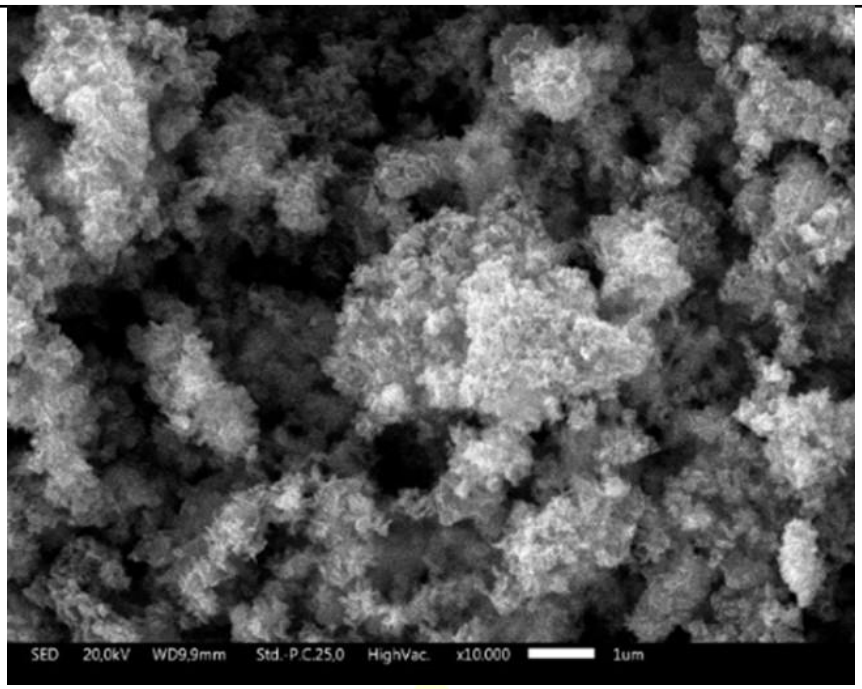

Figure 3.1: SEM image 10,000× of metal-oxide nanostructures for photocatalytic pollutant degradation scale bar: 1 µm.

The study emphasized on using light-driven catalytic processes to degrade harmful organic pollutants using nanostructured metal oxides. Scanning Electron Microscopy SEM is crucial for this study because it offers comprehensive information about the surface characteristics and morphology of the nanostructures. With a 10,000x magnification and a 1 µm scale bar, the SEM image that is part of the data enables researchers to look at the size, shape, and structural characteristics of the metal-oxide nanomaterials, such as nanoparticles, nanowires, or porous frameworks. Since high surface area and individualized porosity improve light absorption and pollutant adsorption, these physical features have a direct impact on photocatalytic performance. While the standard detector Std.-P.C.25.0 records topographical details essential for measuring material quality, the 20.0 kV accelerating voltage ensures high-resolution imaging. The study can optimize the synthesis of these nanostructures and make sure they have an appropriate morphology for maximum degradation activity by contrasting SEM data with measurements of photocatalytic efficiency. Furthermore, SEM can be used together with Energy-Dispersive X-ray Spectroscopy EDS to confirm the elemental composition, detect impurities, and confirm the presence of significant metal oxides such as ZnO or TiO_2. Everything considered, SEM is a crucial instrument in this study, bridging the gap between the functional application of nanostructure design in environmental remediation and its design.

3.2 FTIR

Significant molecular-level insights into the photocatalytic degradation of organic pollutants mediated by metal-oxide nanostructures can be acquired from the analysis of Fourier Transform Infrared FTIR spectroscopy. The spectrum shows a number of unique vibrational modes that together clarify the photocatalytic system's mechanistic characteristics. O-H stretching vibrations can be determined by their broad and strong absorption bands in the 3519–3399 cm^{-1} range, which have transmittance values between 70 and 72%. Both physically adsorbed water molecules and surface hydroxyl groups -OH chemically bound to the metal-oxide framework are the source of these characteristics. These surface hydroxyls are important

active sites in photocatalysis because they produce highly reactive hydroxyl radicals •OH upon photoexcitation, which are the primary oxidizing species that start the degradation of pollutants.

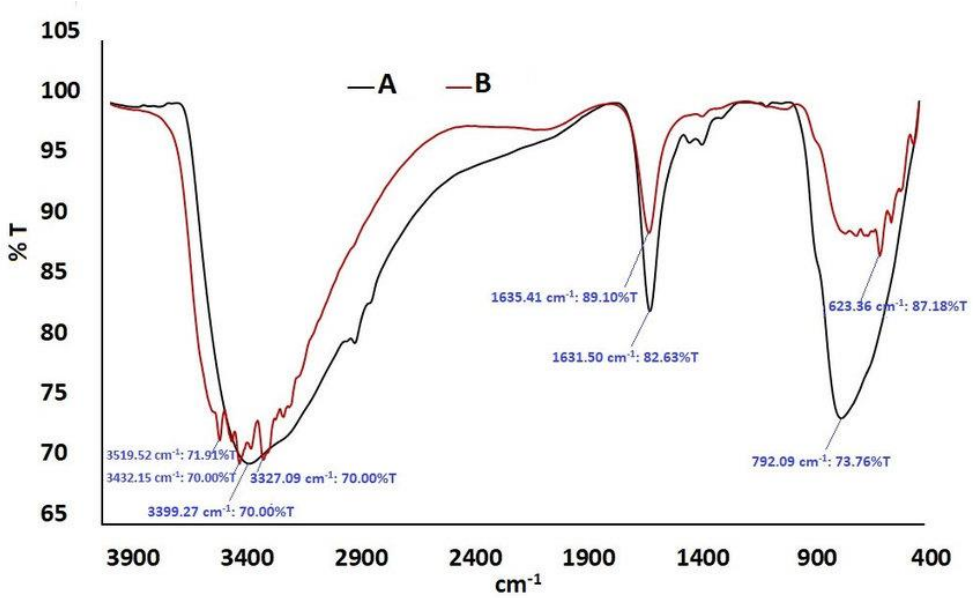

Figure 3.2: FTIR spectrum of metal-oxide nanostructures showing hydroxyl groups 3500–3400 cm^{-1}, organic intermediates 1635 cm^{-1}, and metal-oxygen bonds 792 cm^{-1}.

The H-O-H bending vibration of adsorbed water molecules or C=O stretching modes from carbonyl functional groups are the two possible causes of the pair of medium-intensity peaks seen at 1635 and 1631 cm^{-1} with transmittance values of 89.10% and 82.63%, respectively. Because it suggests the creation of intermediate oxidation products during the photocatalytic degradation process, the latter interpretation is especially significant. These could be carboxylic acids, ketones, or aldehydes that develop as organic pollutants gradually decrease due to oxidation. Direct spectroscopic proof of the current photocatalytic mineralization process can be demonstrated by the presence of such intermediates. A fingerprint region absorption characteristic of metal-oxygen M-O lattice vibrations is expressed by the sharp peak at 792 cm^{-1} 73.76% transmittance. This characteristic demonstrates the material's stability under operating conditions by providing that the metal-oxide's crystalline structure was maintained throughout the photocatalytic reaction. Even though the metal-oxide framework takes part in several redox cycles during photocatalysis, the lack of important peak shifts or new absorptions in this region indicates that it remains intact. Collectively, these spectroscopic signatures present a complete picture of the photocatalytic mechanism: 1 organic pollutants first adsorb onto the metal-oxide surface, which is rich in hydroxyls; 2 photogenerated charge carriers interact with the adsorbed oxygen and surface hydroxyls to produce reactive oxygen species; 3 these radicals systematically attack and degrade pollutant molecules through intermediate carbonyl-containing compounds; and 4 the metal-oxide catalyst maintains its structural integrity throughout the process. By connecting the gap between the material's chemical characteristics and photocatalytic performance, the FTIR data is a powerful diagnostic tool that offers essential insights to enhance the nanostructured photocatalysts for improved environmental remediation applications.

3.3 UV- Visible Spectroscopy

A thorough understanding of the photocatalytic degradation process of organic pollutants using TiO_2 nanostructures is provided by the UV-visible

spectroscopy data presented here. The slow decomposition of organic pollutants is evident from the time-dependent absorbance spectra 0-150 minutes, as shown by the declining absorption intensity in the visible light range of 500-800 nm. The degradation of the pollutants' chromophoric groups corresponds precisely with this decrease in absorbance, demonstrating the TiO_2 photocatalyst's efficacy. The degradation demonstrates a systematic pattern, according to the spectra, with the most notable modifications taking place during the first 60 to 90 minutes of irradiation and a more gradual decline at afterwards points.

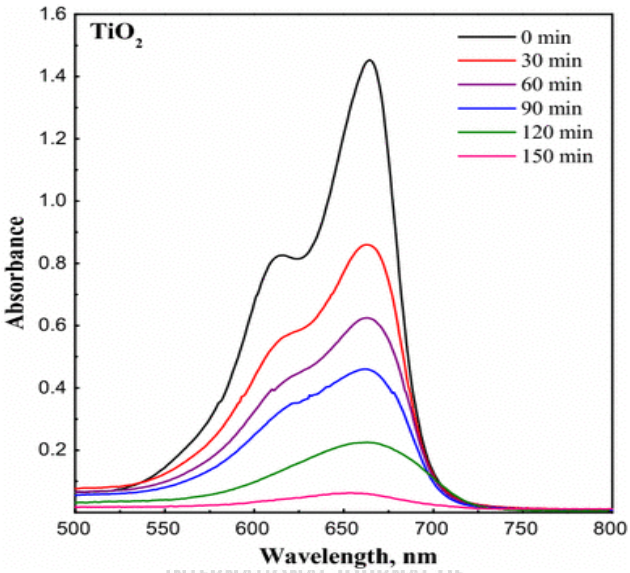

Figure 3.3: UV-Vis absorbance spectra showing time-dependent degradation of organic pollutants by TiO_2 nanostructures 0–150 min. Decreasing absorbance confirms photocatalytic activity.

According to this kinetic profile, there may be a rapid degradation phase at the catalyst surface when there are many pollutant molecules present, which is followed by slower removal rates as the reaction proceeds and the concentration of the pollutants decreases. The wide absorption characteristics in the visible spectrum 500–800 nm are especially significant because they indicate that the TiO_2 nanostructures might have been altered to demonstrate visible-light photocatalytic activity, which is an essential benefit for real-world solar energy applications. The complete mineralization of pollutants without a notable accumulation of colored intermediates is indicated by the lack of new absorption peaks. All of these findings show that TiO_2 nanostructures act as efficient photocatalysts that can break down organic pollutants when exposed to light, and the UV-Vis spectra offer measurable proof of the efficiency and kinetics of the degradation. The data highlights the potential of these metal-oxide nanostructures for environmental remediation applications, particularly for wastewater treatment, where photocatalysis driven by visible light gives important advantages in operation.

3.4 XRD

The presence of crystalline phases, which are crucial to photocatalytic activity, is demonstrated by the intensity peaks seen between 2θ angles of 20° and 60°. While any peak broadening could indicate nanoscale crystallite dimensions consistent with the "nanostructures" referenced in the title the lack of particularly broad peaks indicates that the material has moderate to high crystallinity. The material's bandgap and redox potential are established by the metal-oxide phase such as anatase TiO_2, wurtzite ZnO, or another oxide, which impacts its capacity to degrade organic pollutants under light irradiation. The precise peak positions can aid in identifying this phase. Additionally, the Scherrer equation's

calculation of crystallite size has an enormous effect on photocatalytic performance because smaller crystallites have more surface area suitable for light absorption and pollutant adsorption.

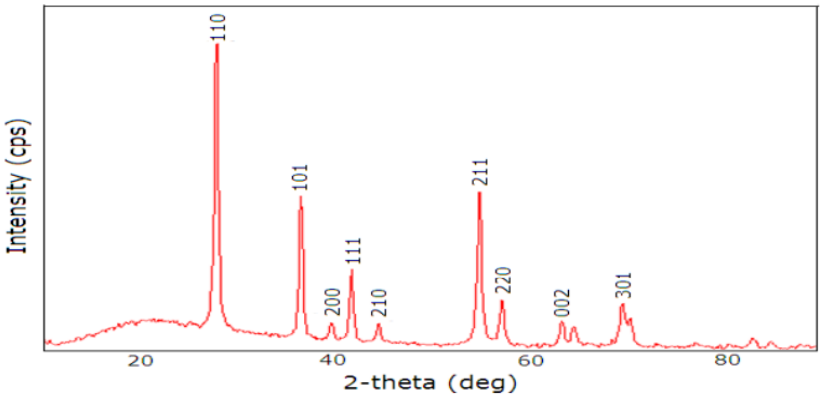

Figure 3.4: XRD pattern of metal-oxide nanostructures used for photocatalytic degradation of organic pollutants. The peaks indicate crystalline phases, while peak broadening suggests nanoscale crystallinity, critical for enhanced photocatalytic activity.

Primary crystalline phases dominate the pattern, however instrumental artifacts or amorphous content may be the cause of noise and negative intensities in the low-angle region below 10° 2θ. In order facilitate material optimization for environmental applications, further XRD data refinement, microscopy, and photocatalytic testing will help correlate the structural characteristics of the metal-oxide nanostructures with their degradation efficiency.

3.5 Photocatalytic Degradation Experiments

The degradation of various organic dyes MB, RhB, and MO under UV or visible light irradiation was employed to evaluate the photocatalytic activity of the synthesized nanostructures.

3.5.1 Experimental Setup

The photocatalytic reactions were carried out in a borosilicate glass reactor that was subjected to either a solar simulator AM 1.5 or a UV lamp 365 nm, 125 W. Throughout the experiment, the catalyst and dye solution were constantly combined via magnetic stirring.

3.5.2 Photocatalytic Procedure

A determined volume of catalyst 0.5–1.0 g/L was added to a dye solution with a known concentration 10–20 mg/L. To establish an adsorption-desorption equilibrium between the catalyst and dye molecules, the suspension was magnetically stirred for half an hour in the dark before being placed under light. Aliquots were subsequently taken out of the reaction at regular intervals e.g., every 10 or 15 minutes while it was exposed to light.

After centrifuging the aliquots in order to remove catalyst particles, the absorbance at the dye's maximum wavelength 664 nm for MB Methylene Blue, for example was measured with a UV-Vis spectrophotometer to calculate the concentration of dye that persisted.

3.5.3 Degradation Efficiency Calculation

The degradation efficiency % was calculated using the following formula:

$$\text{Degradation Efficiency\%} = \left(\frac{C_0 - C_t}{C \cdot 0}\right) \times 100$$

Where

C0= initial dye concentration

Ct= dye concentration at time *t*

Experiments were conducted out with varying catalyst dosages 0.2 to 1.5 g/L, initial dye concentrations varying between 5 and 50 mg/L, and pH values adjusted from 3 to 11 in order to understand the impact of various operating conditions. In order to assess their impact on the overall efficiency of the process, the influence on different irradiation sources

such as UV, visible, and solar light was also looked at. To assess their individual and combined impact on the system's performance, these parameters were systematically shifted, providing insights into the best conditions for maximizing effectiveness.

Recycling experiments were conducted out in order to assess the photo catalyst's stability. The catalyst was recovered, cleaned, and dried after each cycle so that it could be utilized again in later degradation runs. To evaluate a decrease in performance, the efficiency was monitored over three to five cycles.

Prabakaran Eswaran et al 2024 described that the investigation into the photocatalytic activity of ZnO nanoparticles ZnONPs and the ZnO/biochar ZnO/BC nanocomposite for MB dye degradation was carried out through a series of photocatalytic studies. To initiate the experimentation, a stock solution of 0.05 g of MB dye, equivalent to 100 parts per million 100 ppm, was dissolved in distilled water within a standard 1L measuring flask. Subsequently, a quantity of 10 mL from this stock solution, constituting 10 ppm of MB dye, was added to a 100-mL standard measuring flask, wherein it was reconstituted with distilled water. This solution, having the desired concentration, was utilized for the ensuing experiments. The photocatalytic degradation reactions were executed by introducing 100 mg of the photocatalysts into a 100 mL solution of 10 ppm MB dye within a glass beaker. To ensure a well-dispersed mixture and attain an adsorption/desorption equilibrium, the amalgam was stirred in the dark for duration of 30 min. Following this, the suspension was subjected to natural sunlight irradiation. At specific intervals of time, 10 mL of the solution was extracted and subjected to filtration using a 0.45-µM syringe filter to eliminate the presence of photocatalysts.

The collected solution underwent assessment for MB dye concentration using a UV–Vis spectrophotometer. Specifically, the absorbance at 664 nm was examined during the degradation process. This procedure allowed for the continuous monitoring and evaluation of the degradation process over different time intervals of 20 min. The percentage of MB degradation efficiency % was calculated using the following equation 1 [58, 59]:

Degradation efficiency $\eta\% = C0 - Ct \times 100 \div C0$

where C0 and Ct represent the absorbance of MB solution before and after the photocatalytic degradation activity. The said procedure was also used for the dosages, concentrations of MB, pHs, stability, and scavenger studies. The pHs were adjusted by using 0.1 M HCl or 0.1 M NaOH. Degradation kinetic rate constants of MB with ZnONPs and ZnO/BC nanocomposite were evaluated by using the first-order rate equation as given below [60]:

$$I_{nCt \div c_{01}} = -kt$$

where C0 is the initial concentration and Ct is the final concentration before and after irradiation time t. k is the degradation rate constant min^{-1} [30].

3.6 kinetics and mechanism

The provided kinetic plots analyze the degradation mechanism of organic pollutants using metal-oxide nanostructures through pseudo-first-order PFO and pseudo-second-order PSO kinetic models. The left plot, depicting ln $q_e - q_t$ versus time, suggests a PFO mechanism if linear, indicating that the degradation rate depends primarily on the concentration of the pollutant. The slope of this linear fit provides the rate constant k_1, min^{-1}, which quantifies the reaction speed. The right plot, showing t/q_t versus time, tests for PSO kinetics, where a linear trend implies that the process is controlled by chemisorption or surface reactions, with the slope and intercept yielding the rate constant k_2, $g \cdot mg^{-1} \cdot min^{-1}$ and equilibrium adsorption capacity q_e, respectively. The multiple curves for different pollutant concentrations 5–20 ppm reveal how degradation kinetics vary with initial pollutant load, offering insights into the catalyst's efficiency under varying conditions. A stronger fit to the PSO model would suggest that the degradation is dominated by strong interactions between the pollutant molecules and the catalyst surface, a key factor in designing effective photocatalytic systems. This kinetic analysis is crucial for optimizing reaction parameters and improving the nanostructures' performance in environmental remediation applications.

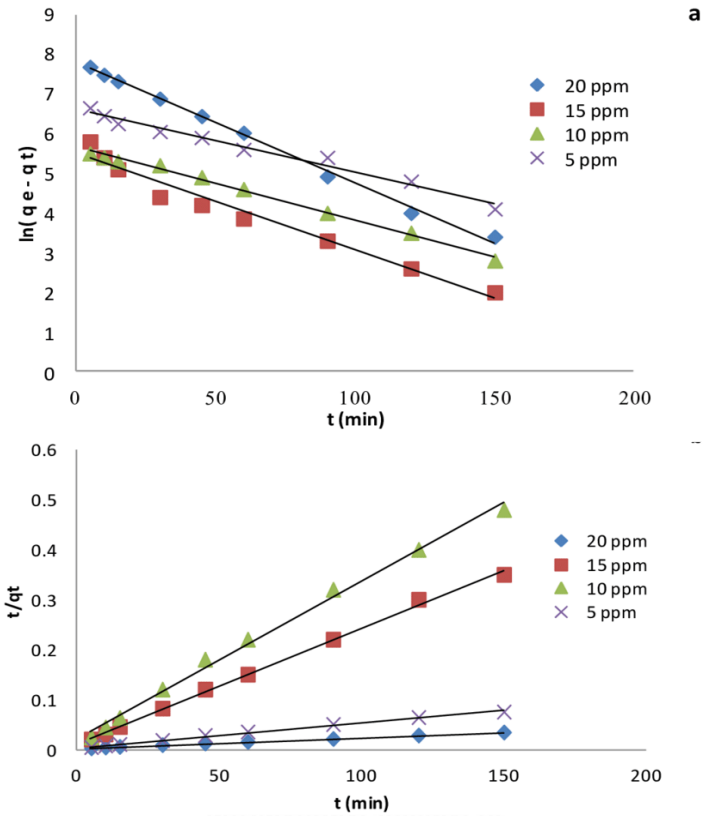

Figure 3.5: Kinetic analysis of photocatalytic degradation: Pseudo-first-order left and pseudo-second-order right model fits for different pollutant concentrations 5–20 ppm.

4 Conclusion and future perspective

TiO_2, ZnO, and FeO_3 are environmentally friendly metal-oxide nanostructures that have been successfully synthesized and applied in this study for the efficient photocatalytic degradation of organic pollutants like methyl orange, rhodamine B, and methylene blue. The structural integrity, surface functionality, and optical activity of the nanomaterials were validated by characterization methods such as SEM, XRD, FTIR, and UV-Vis spectroscopy. Kinetic studies demonstrated a surface-controlled pseudo-second-order reaction mechanism, and the photocatalytic performance, evaluated under a range of operational parameters, demonstrated high degradation efficiency and good reusability. These findings indicate the potential of these nanostructures for environmentally friendly wastewater treatment. To increase their photocatalytic activity in actual wastewater conditions and under visible light, more developments are required. To improve charge separation and light absorption, future studies should investigate the utilization of dopants, heterojunction formation, and green synthesis techniques. To enable industrial applications in water purification technologies, it is also essential to conduct a thorough investigation into long-term stability, environmental impact, and scale-up feasibility.

REFERENCES

[1] "Environmental pollution.," Ceylon Med. J., vol. 17, no. 2, pp. 61–62, 1972.
[2] "Iqbal, M. A., & Gupta, S. G. 2009. Studies on heavy metal ion pollution of ground water sources as an effect of municipal solid waste dumping. African Journal of Basic & Applied Sciences, 15–6, 117–122.".

[3] "Finney, J. L. 2004. Water? What's so special about it? Philosophical Transactions of the Royal Society of London. Series B: Biological Sciences, 3591448, 1145–1165.".
[4] "Ripl, W. 2003. Water: The bloodstream of the biosphere. Philosophical Transactions of the Royal Society of London. Series B: Biological Sciences, 3581440, 1921–1934.".
[5] "Jinwal, A., & Dixit, S. 2008. Pre-and post-monsoon variation in physico-chemical characteristics in groundwater quality of Bhopal 'The City of Lakes' India. Asian Journal of Experimental Sciences, 223, 311–316.".
[6] "Shiklomanov, I. A., & Rodda, J. C. eds., 2004. World water resources at the beginning of the twenty-first century. Cambridge University Press".
[7] "Madhav, S., Ahamad, A., Kumar, A., Kushawaha, J., Singh, P., & Mishra, P. K. 2018a. Geochemical assessment of groundwater quality for its suitability for drinking and irrigation purpose in rural areas of Sant Ravidas Nagar Bhadohi, Uttar Pradesh. Geol".
[8] "ScienceDirect - Food and Chemical Toxicology : The potential for human exposure, direct and indirect, to the suspected carcinogenic triphenylmethane dye Brilliant Green from green paper towels", [Online]. Available: http://www.sciencedirect.com/science/article/pii/S0278691511001931
[9] "Inyinbor Adejumoke, A., Adebesin Babatunde, O., Abimbola, O., & Adelani-Akande Tabitha, A. 2018. Water pollution: Effects, prevention, and climatic impact. Water Challenges of an Urbanizing World, 33.".
[10] "Waters, T. F. 1995. Sediment in streams: Sources, biological effects, and control. American Fisheries Society.".
[11] "Bilotta, G. S., & Brazier, R. E. 2008. Understanding the influence of suspended solids on water quality and aquatic biota. Water Research, 4212, 2849–2861.".
[12] "E. Nazarzadeh Zare, A. Mudhoo, M. Ali Khan, M. Otero, Z.M.A. Bundhoo, M. Patel, A. Srivastava, C. Navarathna, T. Mlsna, D. Mohan, Smart Adsorbents for Aquatic Environmental Remediation, Small. 17 2021 2007840".
[13] "E.N. Zare, A. Motahari, M. Sillanpää, Nanoadsorbents based on conducting polymer nanocomposites with main focus on polyaniline and its derivatives for removal of heavy metal ions/dyes: A review, Environ. Res. 162 2018 173–195".
[14] "E.C. Okpara, O.C. Olatunde, O.B. Wojuola, D.C. Onwudiwe, Applications of Transition Metal Oxides and Chalcogenides and their Composites in Water Treatment: a review, Environ. Adv. 11 2023 100341.".
[15] "J. Hosseini, E.N. Zare, D. Ajloo, Experimental and theoretical calculation investigation on effective adsorption of leadII onto polyaniline-co-pyrrole nanospheres, J. Mol. Liq. 296 2019 111789 1–12.".
[16] "Jayaswal K, Sahu V, Gurjar BR 2018 Chapter 2: Water pollution, human health and remediation. In: Bhattacharya S, Gupta A, Gupta A, Pandey A eds Water remediation. Energy, environment, and sustainability. Springer, Singapore, pp 11–27. https://doi.org/".
[17] "Meenakshisundaram S 2019 Environmental photocatalysis/photocatalytic decontamination. In: Martínez L, Kharissova O, Kharisov B eds Handbook of ecomaterials. Springer, Cham, pp 1625–1640. https://doi.org/10.1007/978-3-319-68255-6_65".

[18] "Monga D, Basu S 2019 Enhanced photocatalytic degradation of industrial dye by g-C3N4/TiO2 nanocomposite: role of shape of TiO2. Adv Powder Technol 305:1089–1098. https://doi.org/ 10.1016/j.apt.2019.03.004".

[19] "Mudassir MA, Hussain SZ, Khan M, Asma ST, Iqbal Z, Huma Z, Ullah N, Zhang H, Ansari TM, Hussain I 2018 Polyacrylamide exotemplate-assisted synthesis of hierarchically porous nanostructured TiO2 macrobeads for efficient photodegradation of organic dyes a".

[20] "Abigail, M.; Samuel, S.M.; Ramalingam, C. Addressing the Enviromental impacts of butachlor and the available remediation strategies: A systematic review. Int. J. Enviro. Sci. Tech. 2015, 12, 4025–4036. [Google Scholar] [CrossRef] [Green Version]".

[21] "Samuel, M.S.; Bhattacharya, J.; Parthiban, C.; Viswanathan, G.; Singh, N.P. Ultrasound-assisted synthesis of metal organic framework for the photocatalytic reduction of 4-nitrophenol under direct sunlight. Ultrason. Sonochem. 2018, 49, 215–221. [Google Sc".

[22] "Samuel, M.S.; Subramaniyan, V.; Bhattacharya, J.; Parthiban, C.; Chand, S.; Singh, N.P. A GO-CS@ MOF [Zn BDCDMF] material for the adsorption of chromium VI ions from aqueous solution. Compo. B Eng. 2018, 152, 116–125. [Google Scholar] [CrossRef]".

[23] "Saleh, I.A.; Zouari, N.; Al-Ghouti, M.A. Removal of pesticides from water and wastewater: Chemical, physical and biological treatment approaches. Enviro. Tech. Inno. 2020, 19, 101026. [Google Scholar] [CrossRef]".

[24] "U. Diebold, 'The surface science of titanium dioxide,' Tulane University, New Orleans, LA 70118, USA, Surface Science, 2003.".

[25] "S. Hore, C. Vetter, R. Kern, H. Smit, A. Hinsch, "Influence of scattering layers on efficiency of dye-sensitized solar cells Solar Energy Materials and Solar Cells, vol. 90, 9, May 2006, p.p. 1176-1188.".

[26] "A. Chemsiddine, H. Jungblut, S. Boulmaaz, 'Investigation of the Nanocluster Self-Assembly Process by Scanning Tunneling Microscopy and Optical Spectroscopy,' The Journal of Physical Chemistry B, vol. 100, 30, July 1996, p.p. 12546-12551.".

[27] "A. Muramastu, T. Sugimoto, X. Zhou, 'Synthesis of uniform anatase TiO2 nanoparticles by gel–sol method, Formation process and size control,' Journal of Colloid and Interface Science, vol. 259, 1, p.p. 43-52, March 2003.".

[28] "Yin Z, Wada Y, Kitamura T, Kambe S, Murasawa S, Mori H, et al. Hydrothermal synthesis of nanosized anatase and rutile TiO2 using amorphous phase TiO2. J Mater Chem 2001;11:1694–703.".

[29] V. Gerbreders et al., "Hydrothermal synthesis of ZnO nanostructures with controllable morphology change," CrystEngComm, vol. 22, no. 8, pp. 1346–1358, 2020, doi: 10.1039/c9ce01556f.

[30] P. Eswaran, P. D. Madasamy, K. Pillay, and H. Brink, "Sunlight-driven photocatalytic degradation of methylene blue using ZnO/biochar nanocomposite derived from banana peels," Biomass Convers. Biorefinery, vol. 15, no. 8, pp. 12347–12367, 2025, doi: 10.1007/s13399-024-05999-z.